12th AIAA International Space Planes and Hypersonic Systems and Technologies
15 - 19 December 2003, Norfolk, Virginia

AIAA 2003-6990

12th AIAA Intl. Space Planes & Hypersonic Systems & Technologies
Norfolk, Virginia, 15-19 December 2003

Characterization of Liquid Fuel Mixing in a Scramjet Flowfield

S. Shani*, T. Tran†, F. Genin†, J. Matlach‡, S. Menon§, J. Seitzman¶

School of Aerospace Engineering
Georgia Institute of Technology
Atlanta, GA 30332-0150

ABSTRACT

This paper describes an experimental program to provide high quality, fuel-air mixing data in a well-characterized scramjet model flowfield for validation of computational tools, such as subgrid LES models. The study employs a noncombusting, supersonic windtunnel and a standard, backward-facing step configuration that allows injection of gaseous or liquid fuel (or fuel surrogates). The facility is modular, with nozzles for providing flows from M=1.5 to 3.5. The facility is instrumented so as to provide a rigorous set of inlet, boundary, and internal flow properties. Results are presented for a Mach 2.5 flow without injection, and with 90° injection of a nonevaporating liquid fuel surrogate (acetone) just upstream of the step. The results include vertical profiles of inlet Mach number and static pressure; test section, wall static pressures; downstream profiles of flow static pressures; characterization of the droplet distributions produced by the fuel atomizer; and initial characterization of the fuel mixing as measured by laser-induced fluorescence images. The results are used to characterize the main flow features, such as the expansion over the step, boundary and shear layers and the reattachment shock. The results are repeatable, demonstrating the reliability of the facility. In addition, the liquid injection has little effect on most of the flow features, with results for this case nearly identical to the noninjection case.

INTRODUCTION

An important hurdle in the development of successful hypersonic, air-breathing vehicles is the design of efficient propulsion systems, specifically scramjets. A renewed interest in scramjet-type engines is arising as dual mode ramjet/scramjet configurations are more and more actively investigated.[1,2] The main issues inherent to supersonic combustion arise from the very low residence times in these combustors, and the consequent needs for fast and efficient mixing of fuels and oxidizers. Also, anchoring the flame within the engine is a necessary condition for stable, steady combustion.[1] The backward-facing step configuration, one of the simplest designs, provides both a self-excited resonance, which tends to enhance the mixing process, and a subsonic recirculation zone immediately downstream of the step, which can be used to anchor the flame.[1]

This backward-facing step configuration has been extensively studied for gaseous fuels. [3] Historically, hydrogen has been the primary fuel choice, due to its high amount of chemical energy release. However, the two major drawbacks of this fuel are: 1) the necessity for cryogenic storage, and 2) its very low density. Therefore hydrogen-fueled engines have significant drawbacks in certain hypersonic propulsion, military applications, and in reusable first stages for space launchers.[2] The alternative is the use of liquid hydrocarbon (HC) fuels. While liquid HC fuels are less energetic, they are easier to store, denser, more readily obtainable, and could be used to cool critical structures in hypersonic vehicles.[3-5] Scramjet engines with liquid HC fuels are thus an important option for future supersonic/hypersonic propulsion systems.

Because of the difficulty in recreating the high-enthalpy flight conditions associated with these vehicles, the development and optimization of scramjet designs relies significantly on the creation of accurate computational tools, such as modeling based on Large Eddy Simulations (LES).[6,7] Successful application of such computational methods in scramjet flowfields requires that the computational tools physically and accurately model the various processes that the fuel and air undergo in the combustor. Development and validation of these models, in turn, requires high quality experimental data.

In this vein, this paper presents initial results of an experimental study carried out to produce high quality, fuel-air mixing data for validation of computational models (e.g., subgrid LES models) in a relevant, but achievable flow. The fuel-air mixing problem is a critical one for scramjet combustors. The study eventually will address mixing associated with both gaseous and liquid fuel injection systems. The current paper is limited to mixing of a nonevaporating liquid fuel in a scramjet combustor model flow, with a combustor Mach number (M) of 2.5.

*Visiting Research Engineer, Member AIAA, on sabbatical leave from Rafael-Israel
†Graduate Research Asst., Student Member AIAA
‡Undergraduate Research Assistant, Student Member AIAA
§Professor, Associate Fellow AIAA
¶Associate Professor, Associate Fellow AIAA

EXPERIMENTAL APPARATUS

In order to create a data set of sufficient quality for development and validation of computational models, one must address a number of issues. It requires a flow facility that: 1) sufficiently recreates essential features of the flow environment; 2) runs with well-defined and repeatable conditions; 3) allows flexibility in varying the conditions; and 4) permits accurate measurement techniques to be employed. In addition, the data must include measurements of the inlet and boundary conditions so that the computations can be initiated properly. Finally, measurements of internal and exit flow properties are required to test the predictions of the computational model and provide data for model improvements. The following sections describe the development of the flow facility and the measurement techniques employed.

FLOW FACILITY

The flow facility is a blow down wind tunnel with a backward facing step (Figure 1). Air for the operation of the wind tunnel is compressed up to 18 MPa (2600 psia) by a reciprocating compressor (Norwalk). The air is dried to a dew point of 4.4°C (40°F) at 17.3 MPa (2500 psi, or equivalently -78.9°C at atmospheric pressure) by a refrigerated air dryer before delivery to the storage tanks with a capacity of 2250 m^3 (90,000 scf), which can be recharged in four hours by the compressor.

The wind tunnel can operate at stagnation pressures 0.1-1.4 MPa and stagnation temperatures of 290-420 K. Air preheating is accomplished through an indirect, gas-fired heat exchanger. Based on the ability to maintain the reservoir stagnation pressure, maximum run times for the wind tunnel are 5-15 minutes depending on the Mach number, though individual tests can usually be completed in less than 1-2 minutes. For these short runs, ~10-20 tests can be carried out per day.

The wind tunnel is located in a high-pressure test bay, and is operated remotely from a safe control room. A pressure indicating controller located within the control room allows the operator to set the desired pressure delivered to the wind tunnel. This controller commands a set of three control valves designed to maintain steady flow at the desired outlet pressure over a range of inlet pressures as the storage tanks discharge. Pressure feedback is provided to the controller by a 6.9 MPa (1,000 psi) pressure transmitter. The air supply system is capable of reaching stable operating conditions in less than 20 seconds and provides inlet pressures constant to within 6.9 kPa (1 psi). The air is delivered to the test bay through a 20 cm (8 inch) diameter pipe, and then to a turning section (Figure 1) by a 15 cm (6 inch) diameter pipe. The turning section is required due to the location of the air supply and exhaust systems of the high pressure test lab. It also acts as a low velocity, upstream reservoir for monitoring the flow stagnation conditions.

Upon leaving the reservoir, the air moves through two coarse screens to reduce turbulence levels, two honeycomb flow straighteners, and, finally, several more turbulence reducing screens before entering the converging/diverging nozzle and the optically accessible test section (see Figure 1).

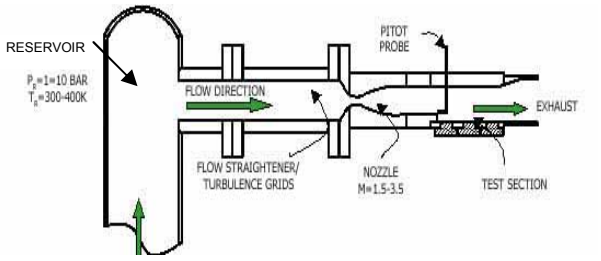

Figure 1. Schematic of supersonic wind tunnel assembly.

The supersonic wind tunnel is constructed in a highly modular fashion allowing great flexibility of tests and measurements within the test-section. Three interchangeable, two-dimensional nozzles were designed using a method of characteristics approach. The nozzles were designed to produce M=1.56, 2.5 and 3.5 flow conditions. The top and bottom sections of the nozzles are contoured while the sides are flat; therefore, the boundary layers are essentially two-dimensional. The compute nozzle profiles were designed to account for boundary layer growth on the top and bottom. No attempt was made to correct the counter surface to account for boundary layer growth on the nozzle sidewalls. A more complete description of the coordinates of the contours of the 30 cm long, Mach 2.5 nozzle and the 34.5 cm, Mach 3.5 nozzle are described elsewhere.[8]

The inlet section, between the nozzle and the test section, has a cross section of 80×83.4 mm and a length of 10 cm, while the cross section of the test section is increased to 80×108 mm behind the rearward facing step. The two sidewalls of the test-section are fitted with optical grade, quartz windows (23.5 cm long), allowing for the unobstructed observation of the entire height and length of the test-section (Figure 2).

The entrance of the test section follows a rearward-facing step geometry commonly employed in scramjet studies. The step (height h=24.6 mm) can be used as source of axial as well as normal fuel injection, while transverse injection can be performed through the bottom of the test section, downstream of the step. Note, throughout this paper, all measurements locations are defined using the bottom of the step as the origin (see Figure 2). In addition, the test section incorporates six measurement ports (3 in the top wall and 3 in the

bottom). The locations of the ports, as well as the dimensions of the tunnel are shown in Figure 3.

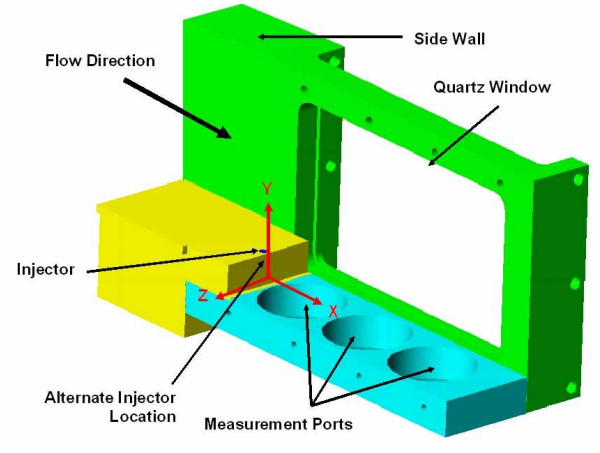

Figure 2. 3-d cutaway view of the of test section; the locations of the bottom test ports and the step are shown, also included is the coordinate system used throughout the paper.

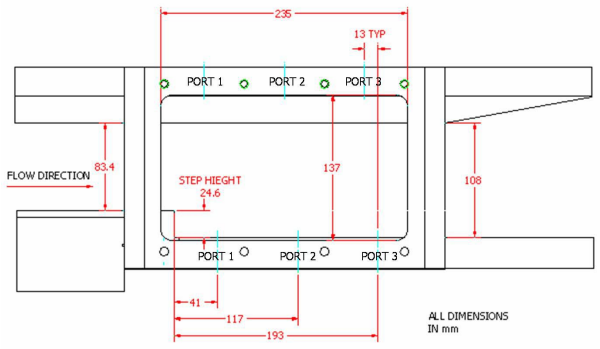

Figure 3. Test section dimensions.

INJECTION SYSTEM

"Fuel" (or more properly a fuel marker) can be introduced into the flow at various locations. For liquid fuel studies, axial injection would occur from the downstream side of the rearward-facing step, while transverse injection is from a location in the top of the step, just upstream of the step. The possibility also exists for injection downstream of the step from one of the test ports. The spray emitting from the injector should be compatible with the two-dimensional nature of the flow. Thus the distribution from the injector should at least be transversely symmetric about the centerline of the tunnel.

As noted below, acetone is used as the fuel marker. The acetone is injected through a fine atomizing spray injector (Hago Manufacturing Co., model M1), which is designed to create a solid cone spray pattern with an 80° full angle (see Figure 4) when supplied at 0.69 MPa (100 psi). At this supply pressure, the acetone mass flow rate was measures to be 0.95 gram/sec (0.90 gph). The supply system of the liquid acetone is a tank pressurized using nitrogen gas (maximum pressure of 2.8MPa/400psi). The liquid supply to the injector is controlled by a solenoid valve, connected to a remote switch in the control room. In the present studies, injector is mounted in the top face of the step, at the centerline (Z=0) and 6 mm upstream of the step (X/h=–0.24). The exit of the injector is flush with the top face of the step (see Figure 4).

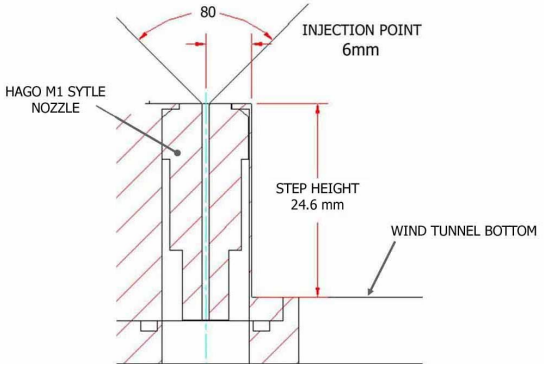

Figure 4. Schematic of liquid fuel injector mounted in the upper side of the step.

MEASUREMENT CAPABILITIES

In order to characterize the quality of the flow within the test-section, pressure and temperature measurements can be taken simultaneously at numerous locations along the walls of the test facility. In addition, a traverse system enables the measurement of pressure and temperature (vertical) profiles at various locations upstream and downstream of the step. The measurements are recorded with a 16-channel, computerized data acquisition system and a custom (Labview) interface, typically with a sampling rate of 1kHz. Finally, two imaging techniques are used. Schlieren imaging is used to identify flow features. Planar laser-induced fluorescence (PLIF) allows characterization of the fuel distribution and mixing in the facility.

PRESSURE MEASUREMENTS

Tunnel stagnation pressures are measured in the reservoir section, and they can also be obtained just upstream of the nozzle in the settling chamber. Static pressures can be measured at seven static pressure ports located along the sidewall of the nozzle (at the vertical centerline). As noted above, there are three test ports located in each of the top and bottom walls of the test section walls (Figure 2). Each port can be fitted with plugs installed flush with the top and bottom surfaces of the test section for the measurement of static pressures. Each static pressure plug has 33 static pressure taps configured in a plus sign. Thus from each

plug, static pressure measurements can be obtained at 17 axial (X) positions along the test section centerline (Z=0) and another 17 at different transverse (Z) locations with the axial locations defined by the center of the port. With the three plugs installed, static pressures can be measured at 51 streamwise locations.

Vertical (Y) profiles of the air flow pressures are obtained (nonsimultaneously) by separate static and pitot probes manufactured from a previous design.[8] The probes, both L-shaped, are designed such that both the static and stagnation pressures are acquired at the same flow position. The static probe has its ports located on the left and right sides such that variations in the vertical components of the velocity do not significantly impact the static pressure measurements.

Several types of pressure transducers were used for the various measurements; each has a 1% full scale accuracy. Upstream stagnation pressures in the reservoir and flow straightening sections were measured with absolute 0-200psi/1.4MPa and 0-100psi/0.69MPa pressure transducers. Wall static pressures were measured with either differential transducers (±15psi/0.1MPa) or absolute (0-50psia/0.34MPa) transducers. The pressure of the static probe was monitored with the differential transducers (±15psi/0.1MPa). The stagnation probe pressure was measured with an absolute (0-50psia/0.34MPa) transducer. All pressure data upstream of the nozzle and all wall pressure measurements are averages of 5000 samples recorded over 5 seconds. Traverse pressure results are averaged over 0.5 seconds (500 samples).

TEMPERATURE MEASUREMENTS

Temperatures are measured at several locations along the wind tunnel. Stagnation temperatures are measured in the reservoir section and just upstream of the nozzle in the settling chamber. The surface temperature of the windtunnel, just upstream of the injection point, is measured by a thermocouple embedded ~1mm under the inside face of the bottom wall of the inlet section. Finally, vertical temperature profiles in the air flow just upstream of the step, and at downstream locations are obtained with a sleeved, stagnation temperatures probe,[9] whose configuration is illustrated in Figure 5.

Due to various losses, the temperature measured by the probe (T_{probe}) is not the true stagnation temperature (T_o) of the flow. The probe temperature can be corrected by means of the recovery factor (r), defined by equation (1).[9]

$$\frac{T_{probe}}{T_o} = \frac{\left(1 + r\frac{\gamma-1}{2}M^2\right)}{\left(1 + \frac{\gamma-1}{2}M^2\right)} \qquad (1)$$

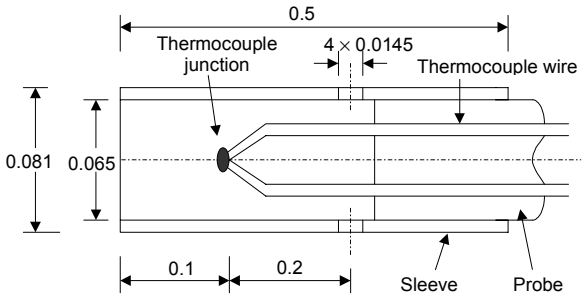

Figure 5. Sleeved thermocouple probe (type T) with exit to inlet area ratio of 20% and bead size of 0.01".

In general, the recovery factor is dependent on the exit to inlet area ratio of the sleeve used in the thermocouple. If this area ratio is too large, the flow does not slow sufficiently for the flow temperature to approach the stagnation temperature. Conversely if the ratio is too small and the internal flow velocity is too low, the response time of the probe and the heat losses to the sleeve increase. In order to identify an optimum exit/inlet area ratio, experiments were performed for different area ratio probes at the center of the test section, where the stagnation temperature is most accurately known (where there has been minimum heat transfer from the walls). A 20% area ratio yielded a recovery factor of 0.96, while a 30% ratio yielded 0.93. Thus, the 20% sleeve was used for all further the temperature measurements

A shielded, type K thermocouple is used to measure the air (stagnation) temperature in the low velocity reservoir. Type T thermocouples are used to measure wall temperature and the probe stagnation temperature. The thermocouple outputs are linearized, temperature compensated and amplified to produce a 1mV/°C analog signal that is fed to the data acquisition system. All temperature results reported here are averaged over 100 samples.

TRAVERSE SYSTEM

The pressure and temperature probes are connected to a traverse mechanism that can be located in any of the top ports of the test section. The probe lengths allow measurements upstream of the step, even though the ports are located downstream. The traverse system consists of a bracket that contain a power screw and a stepping motor. The stepping motor is controlled by the Labview program through an electronic driver that activates the motor. Labview controls the number of steps, the step size, as well the dwell time of the probe at each location. Typically, the step size used was 0.5 mm and a dwell time of 0.5 sec produced 500 samples during each step.

SCHLIEREN

A conventional linear schlieren system is used to visualize the flow structures marked by density gradients, e.g., compression and expansion waves, and boundary and shear layers.[10] A 20-mW red HeNe laser is used as the light source and a razor blade as a knife-edge. The schlieren images are recorded at a high framing rate with an 8-bit, Motionscope (PCI 2000S) high-speed camera (480×420 pixels), capable of operating at up to 2000 frames/sec and a shutter speed of 1/40000 sec. The laser beam passes through a focusing lens and an aperture of 250 μm to improve the beam quality and control the light intensity. Two convex lenses produce an enlarged, collimated beam. The beam passed through the test section of the wind tunnel and is focused using two other convex lenses. The final image is projected onto a ground glass screen, and then recorded by the high-speed camera.

ACETONE PLIF

Planar laser-induced fluorescence (PLIF) of acetone, used as the fuel marker, is used to measure the fuel distribution, and thus the fuel-air mixing. Acetone PLIF was originally developed to measure concentration fields in flows containing acetone vapor.[11] Studies have also recently examined PLIF from liquid acetone for use in two-phase fuel flows.[12]

Here, a pulsed Nd:YAG laser is frequency quadrupled to produce a 266 nm beam with a per pulse energy of 120mJ. The laser beam is formed into a thin, collimated sheet by a set of three cylindrical lenses. The sheet can pass through the quartz windows on the side of the test section, or through smaller windows mounted in the test ports. When the ultraviolet laser sheet comes into contact with the acetone, either liquid or vapor, the acetone fluoresces in the visible (~400-500 nm) range.

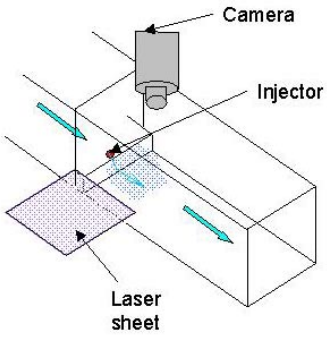

Figure 6. Schematic of PLIF system.

A thinned, backside-illuminated, CCD camera with high quantum efficiency captures the fluorescence, while the glass camera lens (f/1.8) rejects the ultraviolet laser scattering from the droplets, as well as from the windows and walls of the test section. A schematic of the PLIF setup is shown in Figure 6 for top views, with the camera mounted above the test section and the laser entering from the side. The intensity of the fluorescence is a function of concentration of the acetone vapor, and the volume fraction and size of the acetone droplets. Thus, the acetone distribution and the fuel-air mixing can be determined at any location within the flowfield. Note in the cases reported here, the static temperature in the test section is sufficiently low that there should be negligible evaporation of the acetone droplets.

RESULTS

BASE CASE RESULTS

In order to qualify the facility, and provide a base case for computational studies, tests were performed for the Mach 2.5 case with no fuel injection. Figure 7 shows the stagnation temperature measured at the centerline of the inlet, just upstream of the step. (X/h=–0.2 ,Y/h = 1.6, Z/h=0). For reference, the reservoir temperature is also shown. The tunnel flow begins around t=5 s.

The initial temperature spike in the first few seconds is due to warm air initially in the upstream piping. This initial spike changes as the outside (ambient) temperature changes, and it depends on the lapsed time since the air supply was last operated. The difference in the peak temperatures between the reservoir and the freestream is primarily due to the difference in time responses of the two thermocouples (the reservoir thermocouple is slower). The reservoir and freestream temperatures attain nearly steady values after ~10 s, after the warm air passes through the wind tunnel. The difference between the results was used to find the probe's recovery factor (0.96). The steady temperature in the reservoir is slightly below the initial room temperature. As seen here, the wind tunnel can maintain constant temperature operation for at least 40 seconds. For much longer tests (200-300 seconds), the drop in temperature is less than 10°C.

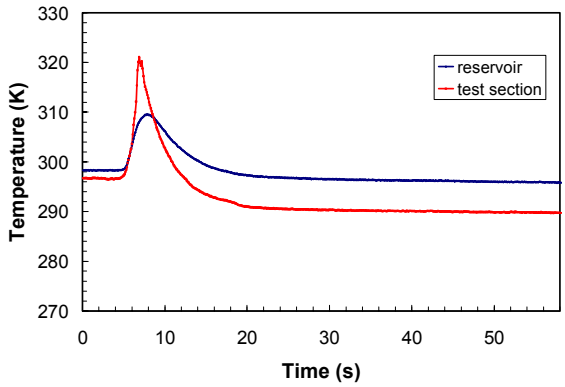

Figure 7. Time traces of the stagnation temperature probe measurement (uncorrected) in the free stream upstream of the step and the reservoir temperature.

The drop in temperature, however, has no measurable effect on the pressure data recorded in the tunnel (pressures remain constants as the temperature drops). When operated at Mach 2.5 with a stagnation pressure of 0.68 MPa (100 psi) and a stagnation temperature of 294 K (70° F), the wind tunnel can operate at the desired pressure conditions continuously for eight minutes (and again the time to achieve stable operation is less than 10-20 seconds. Since most tests, excluding probe traverses, require less than 30 seconds to acquire data, both pressure and reservoir stagnation temperature can usually be considered constant.

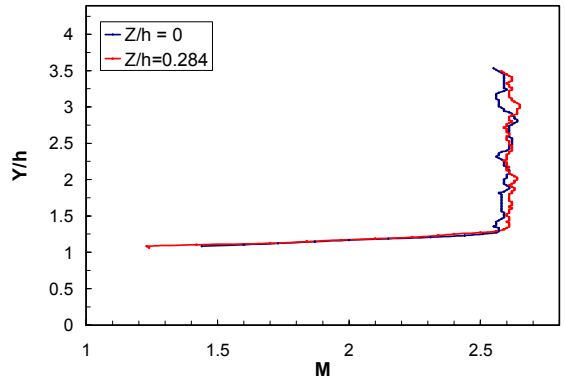

Figure 8. Mach number profiles at the inlet to the test section (X/h = -0.5).

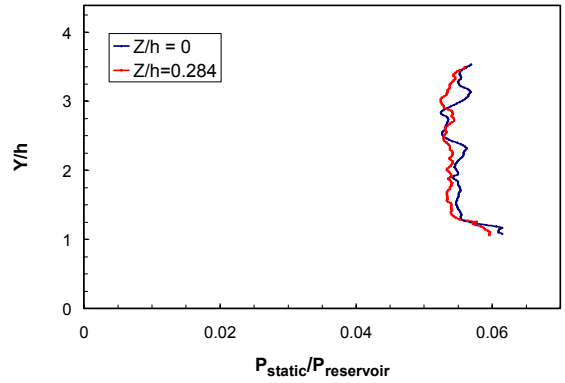

Figure 9. Normalized static pressure profiles at X/h=-0.5.

Figure 8 displays results for the Mach number profile at the inlet of the test section at two transverse locations, centerline and off-center. The Mach number is calculated using the pressure measured from the pitot and static probes according to a standard technique that assumes a calorically perfect gas.[13] The vertical location is normalized to the step height (h=24.6 mm), where zero is taken to be at the floor of the test section. Therefore, Y/h=1 represents the top face of the step. From these results, the boundary layer thickness at the inlet is estimated to be 0.2-0.25h (~5-6mm). The Mach number in the free stream is fairly constant, with an average value of M=2.59 at the centerline and 2.61 at a location 7 mm from the centerline. These values are slightly higher than the design Mach number of the nozzle (M=2.5). The small difference in Mach number for the two transverse locations (<1%) may be attributable to slight errors in the pressure transducer calibrations.

The profiles of the static pressure at the same two locations are shown in Figure 9. The static pressure is normalized to the (~stagnation) pressure in the upstream reservoir, $P_{reservoir}$. The typical value for $P_{reservoir}$ was 0.69 MPa (100 psia). Due to flow losses between the reservoir and the test section, $P_{reservoir}$ is expected to be slightly higher than the stagnation pressure within the test section. A stagnation pressure probe located after the flow straightener section typically shows a 3% loss in stagnation pressure compared to the reservoir. The centerline and off-center profiles are, on average, nearly the same (within 1%).

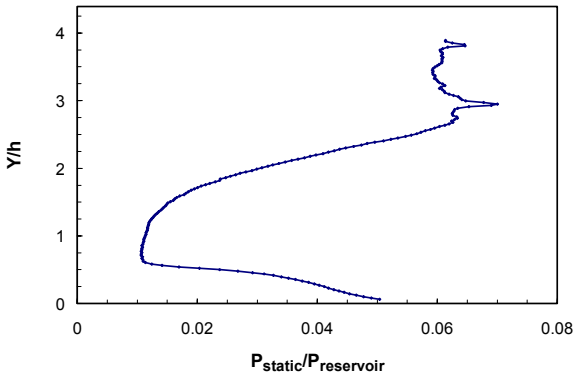

Figure 10. Normalized static pressure profile at X/h=3.0, Z/h=0 (centerline, downstream of the step).

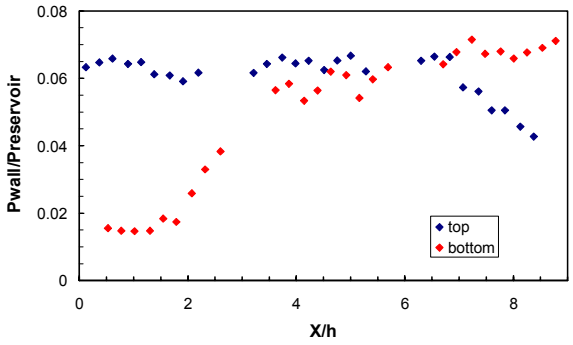

Figure 11. Normalized wall static pressures at Z = 0.

Results obtained in the test section are shown in Figure 10 (static pressure profile downstream of the step) and Figure 11 (static pressures at the top and bottom walls in the test section). The data presented in both figures were repeatable between runs, with deviations generally under 1%. The static pressure profile includes a short section of the freestream

(Y/h>2.9), as well as parts of the flow that have experienced the expansion around the step, the compression due to the bottom wall, and the boundary layer along the bottom wall.

The wall static pressure (Figure 11) also show the effects of these flow features. The static pressure along the bottom walls starts to increase at an axial location of X/h=1.83, which should corresponds to the location where the shear layer reattaches to the wall. The increase in pressure afterward is due to the compression waves created to turn the flow. Assuming the shear layer angle is constant between the step and this point, the shear layer angle is calculated to be 28.6°. The angle of the first expansion fan can also be calculated using the location where the top wall static pressure first starts to decrease. The angle calculated is 24-25°, which is close the theoretical Mach angle of 23° for a Mach 2.6 flow. These two angles were validated by preliminary schlieren images. The location of the bottom of the expansion fan can be also be calculated, if the flow is assumed to expand ideally to the angle of the shear layer. The result is 14°, downward from a horizontal line, and corresponds to a Mach number of 4.13 at the end of the expansion.[13]

From these data and from the traverse static pressure results, we can produce a rough schematic of the characteristics of the test section, as illustrated in Figure 12. This figure helps to further explain the behavior of the static pressure profile shown in Figure 10. Initially, we expected to a region of constant static pressure somewhere above the bottom wall, with gas that had been processed by the reattachment shock. However as seen in Figure 12, the bottom of the expansion fan has already merged with compression waves before the probe location.

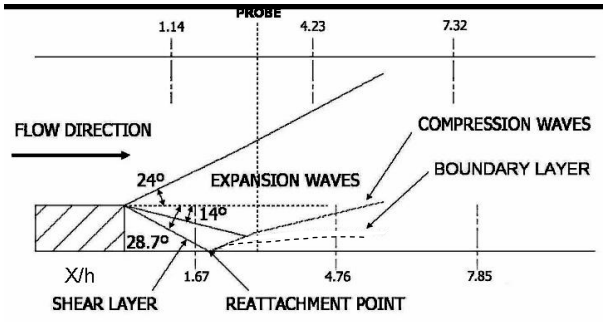

Figure 12. Characteristic flow features (no injection) determined from the wall and traverse static pressures (l traverse location indicated by the line marked "probe").

INJECTION RESULTS

The first set of experiments performed for the fuel injection case were used to characterize the liquid atomizer. A Phase Doppler Particle Anemometer (PDPA) system was used to characterize the M1 Hago nozzle in a separate setup, external to the wind tunnel. Measurements were obtained with the nozzle spraying acetone at a supply pressure of 0.69 MPa. Droplet size and velocity profiles were measured at three different heights above the nozzle exit: 3 mm (⅛ inch), 6 mm (¼ inch) and 13 mm (½ inch). The lowest height data should be a reasonable estimate of the initial conditions of the spray for computational models.

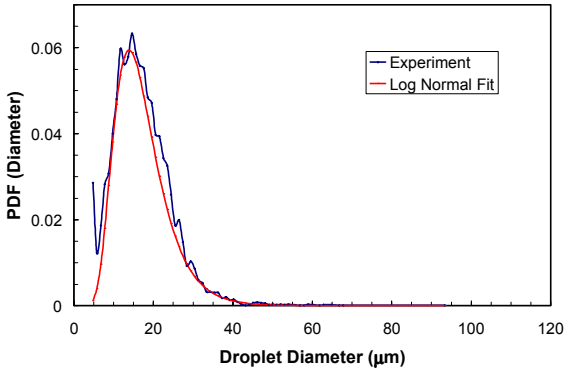

Figure 13. Droplet size PDF of nozzle at one location (Z/h=0, Y/h=0.13), and a log normal distribution fit.

An example of the droplet size distribution is shown in Figure 13 for one location above the nozzle. The results are presented as a probability density function (PDF), and compared to a standard log normal distribution,

$$PDF(D) = \frac{1}{D.\sigma.\sqrt{2\pi}}.\exp\left(-\frac{(\ln(D)-\mu)^2}{2\sigma^2}\right) \qquad (2)$$

where D is the diameter of the droplet, and σ and μ represent the first two moments of the distribution. The distributions agree well, so the complete spray field can be presented assuming log normal distributions.

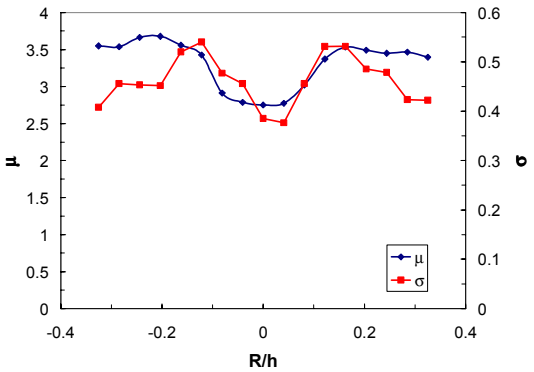

Figure 14. The PDF parameters m and s as a function of radial distance

To this end, the experimental results at each radial location are fit to log normal distributions, and the fit

parameters (μ,σ) are shown in Figure 14 as a function of the radial distance normalized to the step height. It can be seen that the size distribution is nearly symmetric about the centerline, so axisymmetry can be reasonably assumed. Correlations between velocity and droplet size were also obtained, though not presented here.

From the PDF profiles (or the raw data), average droplet sizes can be calculated. Sauter mean diameter (SMD) radial profiles at different heights above the nozzle are shown in Figure 15. Matching profiles of droplet velocity are included in Figure 16. Again, these are the droplet sizes and velocities for no cross flow. The profiles become even more symmetric as the height increases, suggesting the liquid may not have completely finished its break up process at this height. The larger, high velocity droplets could break up and form smaller, slower droplets as they move further away from the nozzle exit, which can be seen in both figures.

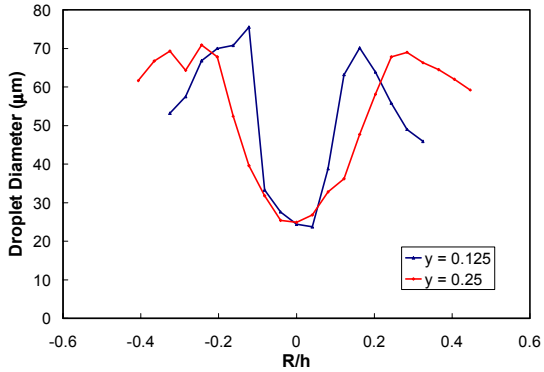

Figure 15. SMD from nozzle at two different heights: y = 0.125, 0.25 inches.

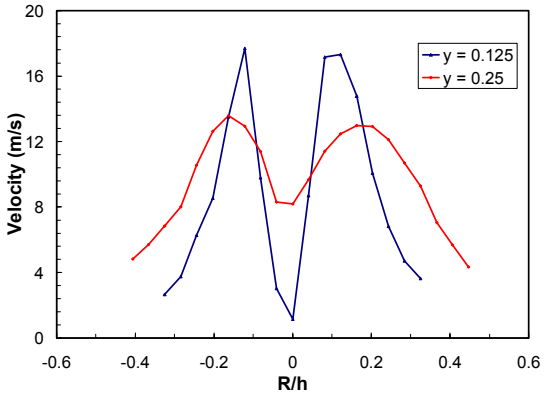

Figure 16. Average droplet velocity as function of radial distance.

The injector was placed in the wind tunnel, and liquid acetone at room temperature was injected into the test section with the injector placed just upstream of the step. Initial measurements of this case have been acquired. Wall static pressure data as well as traverse static pressure were measured and can be compared to the non-injection case.

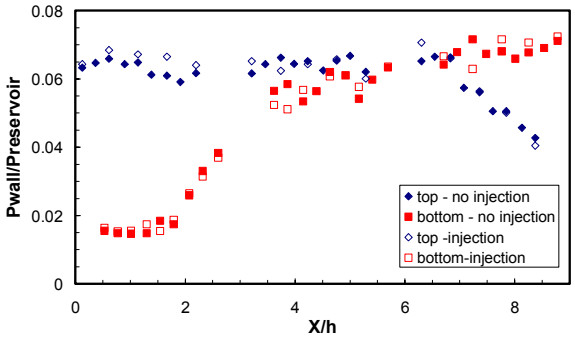

Figure 17. Normalized wall static pressure profile for the injection and non-injection case.

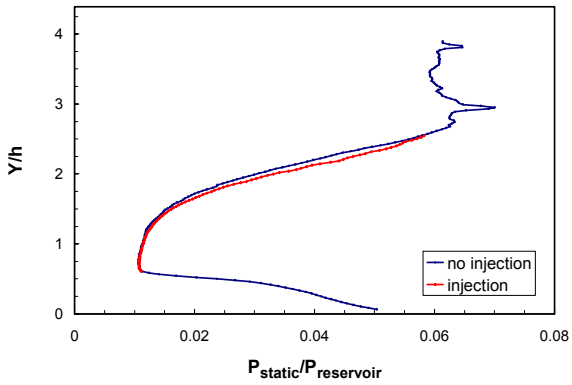

Figure 18. Normalized traverse static pressure at X/h = 3.0 downstream of step for non-injection and injection case.

Figure 17 and Figure 18 show the profiles of the normalized wall static pressure and the traverse static pressure of both the injection and non-injection cases at X/h = 3.0. From both figures, we can see that injection of acetone into the test section has minimal effect upon the static pressure at the wall and the pressure profile in the test section. Data below ~Y/h=0.5 are not included for the injection case. The probe results there displayed a behavior that suggests there may be some influence of the droplets on the probe. Further investigation is ongoing.

Initial results from the PLIF imaging have also been obtained. For the low static temperatures in the test section, the acetone is not expected to evaporate. In fact, the temperature drops below the freezing point of acetone. Heat transfer calculations suggest, however, that even the small droplets will not approach the freezing point until they have traveled well beyond the exit of the test section.

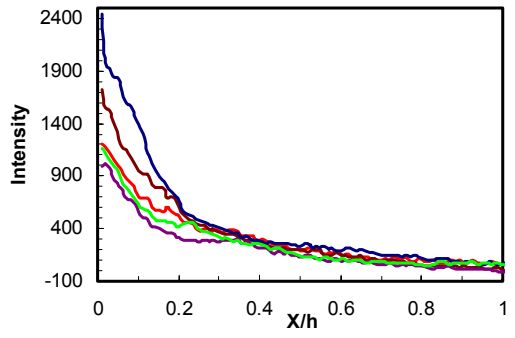

Figure 19. Instantaneous intensity plots of PLIF images, 1mm above step taken at five different times.

Figure 19 shows background corrected, axial profiles of the PLIF data with the laser sheet monitoring a plane ~1mm above the step (Y/h=1.04). Results of five instantaneous realizations are included. The acetone concentration is high near the step, close to the injection point and rapidly decays downstream. The presence of liquid fuel well downstream (X/h>0.5) suggests that at least some of the fuel penetrates through the boundary layer (Y/h=1.2) and into the supersonic freestream. This acetone will then travel some distance downstream before being turned downward by the expansion and returning to the measurement plane location (Y/h=1.04).

Most of the acetone, however, is be expected to be caught in the boundary layer, and thus more closely follow the shear layer. This is confirmed in data taken at a sheet location 5 mm below the step (Y/h=0.8). Most of the acetone does not extend beyond ~X/h=0.4-0.5. This is the location where the shear layer should be from the previous results (e.g., Figure 12). There is, however, a significant amount of acetone in the region just downstream of the step. A possible reason for this is that some of the acetone is entrained into a small recirculation zone behind the step.

SUMMARY

An experimental facility has be created to provide high quality, fuel-air mixing data in a well-characterized scramjet model flowfield for validation of computational tools, such as subgrid LES models. The facility is a noncombusting, supersonic windtunnel (M=1.5-3.5) with a standard, backward-facing step configuration at the inlet to the test section. The facility allows injection of gaseous or liquid fuel at a number of locations. The facility is instrumented so as to provide a rigorous set of inlet, boundary, and internal flow properties. Measurement capabilities include vertical profiles of inlet Mach number, static pressure and stagnation temperature; inlet wall surface temperature; test section, wall static pressures; downstream profiles of flow static pressures and Mach number; characterization of initial droplet distributions produced by the fuel atomizer; schlieren imaging; and characterization of both liquid and gaseous fuel mixing (and evaporation) as measured by planar laser-induced fluorescence.

A complete set of results has been obtained for a Mach 2.5 flow without injection as a base case for comparison to future computations. The results include main flow characteristics, such as the angles for the expansion over the step, boundary and shear layers thicknesses, and the compressions produced by the shear layer reattachment. The results are repeatable, demonstrating the reliability of the facility.

Initial results for liquid acetone injected at 90° just upstream of the step indicate the fuel injection has little effect on most of the flow features, with results for this case nearly identical to the noninjection case. Most of the liquid fuel is contained in the shear layer, though some penetrates the boundary layer.

More extensive measurements will be obtained for the M=2.5 injection case, including temperature profiles, downstream Mach number profiles, and extensive schlieren and PLIF imaging to characterize the fuel mixing. In addition, measurements will be obtained for heated inlet flows, to allow fuel evaporation, and at different Mach numbers.

ACKNOWLEDGEMENTS

This work is supported by NASA through a URETI award (Institute for Future Space Transport). The authors would like to acknowledge the many helpful contributions of D. Scarborough, K. Balakhrishnan, S. Lee and C. Chu.

REFERENCES

[1] Seiner, J. M., Dash, S. M., Kenzakowski, D. C., "Historical Survey on Enhanced Mixing in Scramjet Engines", Journal of Propulsion and Power, v 17, n 6, Nov/Dec, 2001, pp. 1273-1286.

[2]Waltrup, P. J., "Upper Bounds on the Flight Speed of Hydrocarbon-Fueled Scramjet-Powered Vehicles," Journal of Propulsion and Power, Vol 17, No 6, Nov-Dec 2001, pp. 1199-1204.

[3] Curran, E. T. and Murthy, S. N. B., *SCRAMJET Propulsion*, Progress in Astronautics and Aeronautics, Vol. 189, pp. 13-17.

[4] Mathur, T., Lin, K. C., Kennedy, P., Gruber, M., Donbar, J., Jackson, T., and Billig, F., "Liquid JP-7 Combustion in a SCRAMJET Combustor", AIAA 2000-3581, 2000.

[5]Owens, M. G., Tehranian, S., Segal, C., Vinogradov, V. A., "Flame-Holding Configurations for Kerosene Combustion in a Mach 1.8 Airflow," Journal of Propulsion and Power, Vol. 14, No 4, July-August 1998, pp.456-461.
[6]Zeman,O (1993), "A New Model for Super/hypersonic Turbulent Boundary Layers," AIAA paper 93-0897.
[7]Erlebacher, G., Hussaini, M. Y., Speziale, C. G., Zang, T.A., "Toward the large-eddy simulation of compressible turbulent flows," Journal of Fluid Mechanics, Vol. 238, pp. 155-185.
[8] Menon, S. and Fernando, E., *An Experimental/ Numerical Study of Mixing Enhancement in Scramjet Combustors*, report no. WL-TR-91-2077, Wright Laboratory, October 1991.
[9]Michalski, L. et al. *Temperature Measurement*, 2nd ed., John Wiley, New York, 2001.
[10]Settles, G.S., *Schlieren and Shadowgraph Techniques: Visualizing Phenomena in Transparent Media*, Springer-Verlag, Berlin, 2001.
[11]Lozano, A., "Laser-Excited Luminescent Tracers for Planar Concentration Measurements in Gaseous Jets," HTGL report no. T-284, Stanford University, August 1992.
[12]Ritchie, B, Seitzman, J. M., "Quantitative Acetone PLIF in Two-Phase Flows", paper AIAA-2001-0414 at the 39th AIAA Aerospace Science Meeting, Reno, NV, January 8-11, 2001.
[13] Liepmann, H. W. and Roshko, A., *Elements of Gasdynamics*, Dover Publications, Inc. New York, 1957.